


Crystal structure of niraparib tosylate monohydrate Form I, (C₁₉H₂₁N₄O)(C₇H₇O₃S)(H₂O)

James A. Kaduk^{1,2} , Anja Dosen³  and Tom N. Blanton³ 

¹Department of Chemistry, Illinois Institute of Technology, Chicago, IL, USA

²Department of Physics, North Central College, Naperville, IL, USA

³International Centre for Diffraction Data (ICDD), Newtown Square, PA, USA

(Received 28 December 2024; revised 05 March 2025; accepted 20 March 2025)

Abstract: The crystal structure of niraparib tosylate monohydrate Form I has been solved and refined using synchrotron X-ray powder diffraction data and optimized using density functional theory techniques. Niraparib tosylate monohydrate Form I crystallizes in space group *P*-1 (#2) with $a = 7.22060(7)$, $b = 12.76475(20)$, $c = 13.37488(16)$ Å, $\alpha = 88.7536(18)$, $\beta = 88.0774(10)$, $\gamma = 82.2609(6)^\circ$, $V = 1,220.650(16)$ Å³, and $Z = 2$ at 298 K. The crystal structure consists of alternating double layers of cations and anions (including the water molecules) parallel to the *ab*-plane. Hydrogen bonds are prominent in the crystal structure. The water molecule acts as a donor to two different O atoms of the tosylate anion and as an acceptor from one of the H of the protonated piperidine ring. The other piperidyl N–H acts as a donor to the carbonyl group of another cation. Surprisingly, there are no cation–anion N–H...O hydrogen bonds. The amide group forms as a N–H...O hydrogen bond to the anion and an intramolecular N–H...N hydrogen bond to the indazole ring. The powder pattern has been submitted to the International Centre for Diffraction Data for inclusion in the Powder Diffraction File™.

© The Author(s), 2025. Published by Cambridge University Press on behalf of International Centre for Diffraction Data. This is an Open Access article, distributed under the terms of the Creative Commons Attribution licence (<http://creativecommons.org/licenses/by/4.0>), which permits unrestricted re-use, distribution and reproduction, provided the original article is properly cited. [doi:10.1017/S0885715625000181]

Key words: niraparib, Zejula, crystal structure, Rietveld refinement, density functional theory

I. INTRODUCTION

Niraparib (marketed under the trade name Zejula) is used to inhibit poly adenosine diphosphate (ADP-ribose) polymerase from repairing cancer cells. Niraparib is considered a maintenance treatment for cancer patients who have received platinum-based chemotherapy. The drug is administered orally and provided as the salt niraparib tosylate monohydrate. The systematic name of the salt is (CAS Registry Number 1613220-15-7) 2-[4-[(3S)-piperidin-3-yl]phenyl]indazole-7-carboxamide 4-methylbenzenesulfonate hydrate. A two-dimensional molecular diagram of niraparib tosylate monohydrate is shown in Figure 1.

X-ray powder diffraction data for Form I of niraparib tosylate monohydrate, Form II, and anhydrous Form III are provided in U.S. Patent 11673877 (Wu et al., 2023; Tesaro and Merck Sharp & Dohme). Diffraction data for forms APO-I and APO-II of niraparib tosylate are reported in U.S. Patent Application 2021/0017151 (Stirk et al., 2021; Apotex). Powder data for Forms I, II, and III of niraparib free base are reported in International Patent Application WO2020/072966 (Stewart et al., 2020). Single crystal structures of niraparib tosylate monohydrate and a co-crystal of niraparib tosylate and L-proline have been reported very recently (Mudda et al., 2024; Cipla).

This work was carried out as part of a project (Kaduk et al., 2019) to determine the crystal structures of large-volume commercial pharmaceuticals and include high-quality powder diffraction data for them in the Powder Diffraction File™ (PDF®; Kabekkodu et al., 2024).

II. EXPERIMENTAL

Niraparib tosylate monohydrate was a commercial reagent, purchased from TargetMol (Batch #T9497), and was used as received. The white powder was packed into a 0.5-mm-diameter Kapton capillary and rotated during the measurement at ~2 Hz. The powder pattern was measured at 298(1) K at the BXDS-WLE Wiggler Low Energy Beamline (Leontowich et al., 2021) of the Brockhouse Diffraction Sector of the Canadian Light Source using a wavelength of 0.819563(2) Å (15.1 keV) from 1.6 to 75.0° 2θ with a step size of 0.0025° and a collection time of 3 minutes. The high-resolution powder diffraction data were collected using eight Dectris Mythen2 X series 1K linear strip detectors. NIST SRM 660b LaB₆ was used to calibrate the instrument and refine the monochromatic wavelength used in the experiment.

The pattern was indexed with N-TREOR (Altomare et al., 2013) on a primitive triclinic unit cell with $a = 7.22904$, $b = 12.77595$, $c = 13.38682$ Å, $\alpha = 88.738$, $\beta = 88.065$, $\gamma = 82.233^\circ$, $V = 1,224.1$ Å³, and $Z = 2$. The space group

Corresponding author: James A. Kaduk; Email: kaduk@polycrystallography.com

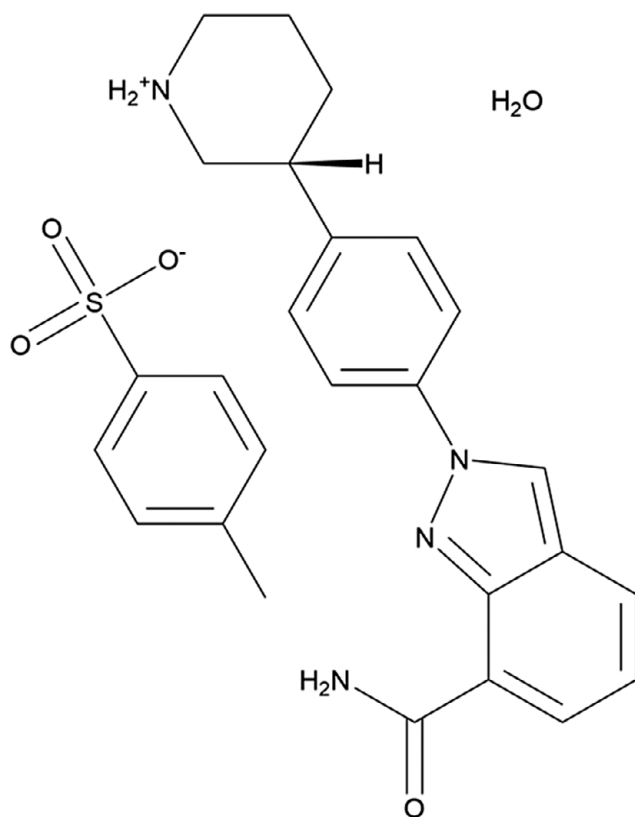


Figure 1. The two-dimensional structure of niraparib tosylate monohydrate.

was assumed to be *P*-1, which was confirmed by the successful solution and refinement of the structure. A reduced cell search of the Cambridge Structural Database (Groom et al., 2016) yielded seven hits but no niraparib derivatives.

The niraparib molecule was downloaded from PubChem (Kim et al., 2023) as Conformer3D_COMPOUND_CID_

24958200.sdf. It was converted to a *.mol2 file using Mercury (Macrae et al., 2020). A tosylate anion was built using Spartan '24 (Wavefunction, 2023). The crystal structure was solved using Monte Carlo simulated annealing techniques as implemented in EXPO2014 (Altomare et al., 2013), using a niraparib molecule, a tosylate anion, and an O atom (water molecule) as fragments, with a bump penalty. Analysis of potential hydrogen bonds (short intermolecular distances) suggested that the amide atom was protonated, so a H atom was added there using Materials Studio (Dassault Systèmes, 2023). This was surprising, as a chemist would expect the amine nitrogen atom in the piperidine ring to be more basic. A similar analysis led to approximate positions of the H atoms on the water molecule along the O...O vectors.

This model was refined using GSAS-II (Toby and Von Dreele, 2013) and optimized using VASP (Kresse and Furthmüller, 1996). The refinement yielded a residual $R_{wp} = 0.05374$ (Figure 2). The root-mean-square Cartesian displacements of the non-H atoms in the Rietveld-refined and VASP-optimized cations and anions were 0.199 and 0.204 Å. The agreement is within the normal range for correct structures (van de Streek and Neumann, 2014). A Mercury Mogul Geometry check (Macrae et al., 2020) indicated that the C–N bond distance of 1.524 Å in the protonated amide was highly unusual (average = 1.314(20) Å; Z-score = 10.4), but that the other geometrical features were normal.

Coincidentally, a single-crystal structure of niraparib tosylate monohydrate has been published by Mudda et al. (2024) – 3 days before we became aware of it. In the Mudda et al. structure, the N atom in the piperidine ring is protonated, as expected. The piperidine ring was modeled as a 50/50 disordered model of two orientations. Each orientation was optimized using VASP. One orientation was 174.308 kJ/mol lower in energy than our model, and the other was 144.397 kJ/mol lower than our model. (The two orientations differed in energy by 29.9 kJ/mol.) The lower-energy orientation based

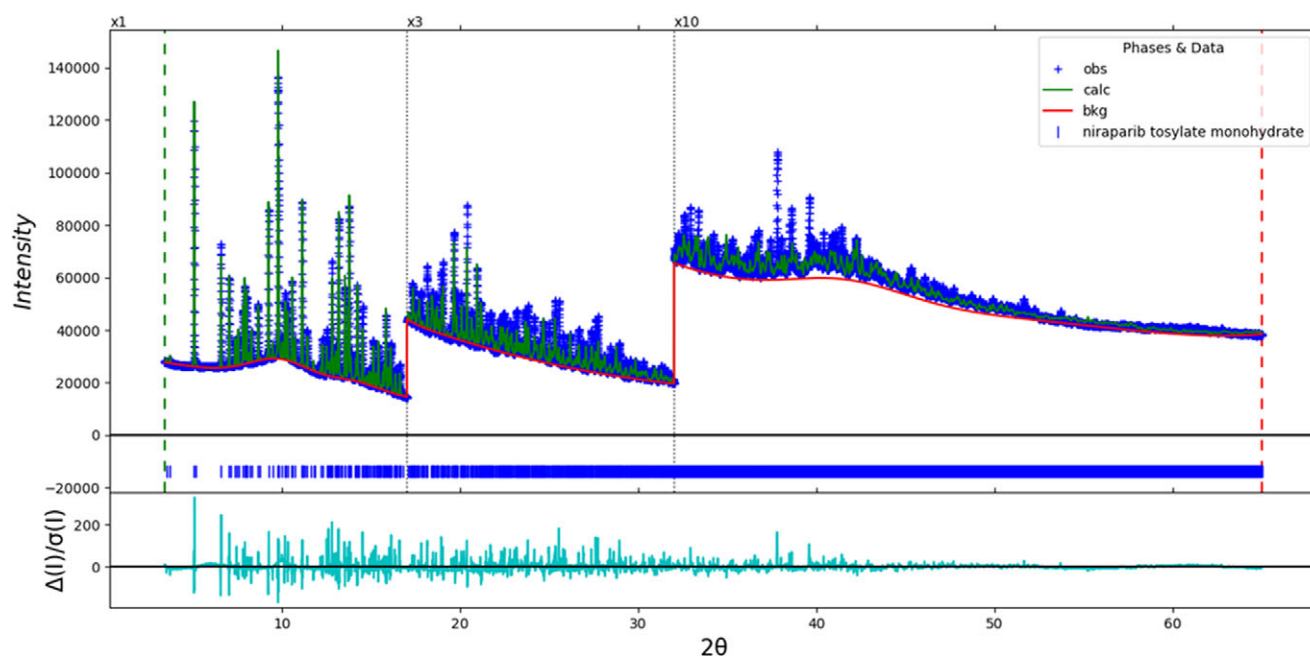


Figure 2. The Rietveld plot for the first refinement of niraparib tosylate monohydrate Form I ($R_{wp} = 0.0537$). The blue crosses represent the observed data points, and the green line is the calculated pattern. The cyan curve is the normalized error plot, and the red line is the background curve. The vertical scale has been multiplied by a factor of $3\times$ for $2\theta > 17.0^\circ$ and by a factor of $10\times$ for $2\theta > 32.0^\circ$.

on the Mudda et al. structure was used to begin another Rietveld refinement on the data in our study.

Rietveld refinement was carried out with GSAS-II (Toby and Von Dreele, 2013). Only the 3.4 to 65.0° portion of the pattern was included in the refinements ($d_{\min} = 0.763 \text{ \AA}$). All non-H bond distances and angles were subjected to restraints, based on a Mercury/Mogul Geometry Check (Bruno et al., 2004, Sykes et al., 2011). The Mogul average and standard deviation for each quantity were used as the restraint parameters. The aromatic rings were restrained to be planar. The restraints contributed 6.7% to the overall χ^2 . The hydrogen atoms were included in calculated positions, which were recalculated during the refinement using Materials Studio (Dassault Systèmes, 2023). The U_{iso} of the heavy atoms were grouped by chemical similarity. The U_{iso} for the H atoms were fixed at 1.3× the U_{iso} of the heavy atoms to which they are attached. The peak profiles were described using the generalized microstrain model (Stephens, 1999). The background was larger and more complex than is typical and was modeled using a six-term shifted Chebyshev polynomial, with broad peaks at 9.90, 14.06, and 41.59° to model the scattering from the Kapton capillary and an apparent amorphous component.

The final refinement of 159 variables using 24,641 observations and 95 restraints also yielded the residual $R_{\text{wp}} = 0.0537$; the two models yielded the same residual, but the second model is more chemically reasonable. The largest peak (1.08 Å from O2) and hole (1.86 Å from C13) in the difference Fourier map were 0.98(22) and $-1.07(22) \text{ e\AA}^{-3}$, respectively. The final Rietveld plot is shown in Figure 3. The largest features in the normalized error plot are in the shapes and positions of some of the low-angle peaks.

The crystal structure of niraparib tosylate monohydrate was optimized (fixed experimental unit cell) with density functional techniques using VASP (Kresse and Furthmüller, 1996) through the MedeA graphical interface (Materials Design, 2024). The calculation was carried out on 32 cores

of a 144-core (768-GB memory) HPE Superdome Flex 280 Linux server at North Central College. The calculation used the GGA-PBE functional, a plane wave cutoff energy of 400.0 eV, and a k -point spacing of 0.5 \AA^{-1} , leading to a $2 \times 1 \times 1$ mesh, and took ~5.4 hours. Single-point density functional calculations (fixed experimental cell) and population analysis were carried out using CRYSTAL23 (Erba et al., 2023). The basis sets for the H, C, N, and O atoms in the calculation were those of Gatti et al. (1994), and the basis set for S was that of Peintinger et al. (2013). The calculations were run on a 3.5-GHz PC using eight k -points and the B3LYP functional and took ~4.3 hours.

III. RESULTS AND DISCUSSION

The experimental powder pattern of niraparib tosylate monohydrate reported by Mudda et al. (2024) does not agree particularly well with that calculated from their crystal structure (Figure 4). The calculated pattern agrees reasonably well with the pattern reported by Wu et al. (2023) (Figure 5), accounting for the fact that the single crystal structure was done at 100 K and the patent pattern measured at ambient conditions and, thus, that the single-crystal cell is smaller. Mudda's experimental pattern can be modeled by assuming a significant preferred orientation (sixth-order spherical harmonics), resulting in a texture index of 5.1. The Bravais–Friedel–Donnay–Harker (Bravais, 1866; Friedel, 1907; Donnay and Harker, 1937) morphology suggests that we might expect elongated morphology for niraparib tosylate monohydrate, with $\langle 010 \rangle$ as the long axis. We suspect that Mudda's experimental pattern was measured from a poor specimen. The pattern from such an oriented specimen might not be useful for phase identification.

The thermal expansion of niraparib tosylate monohydrate between 100 and 298 K is anisotropic (Table I). The expansion along the a -axis is 1.5%, while that along the b - and

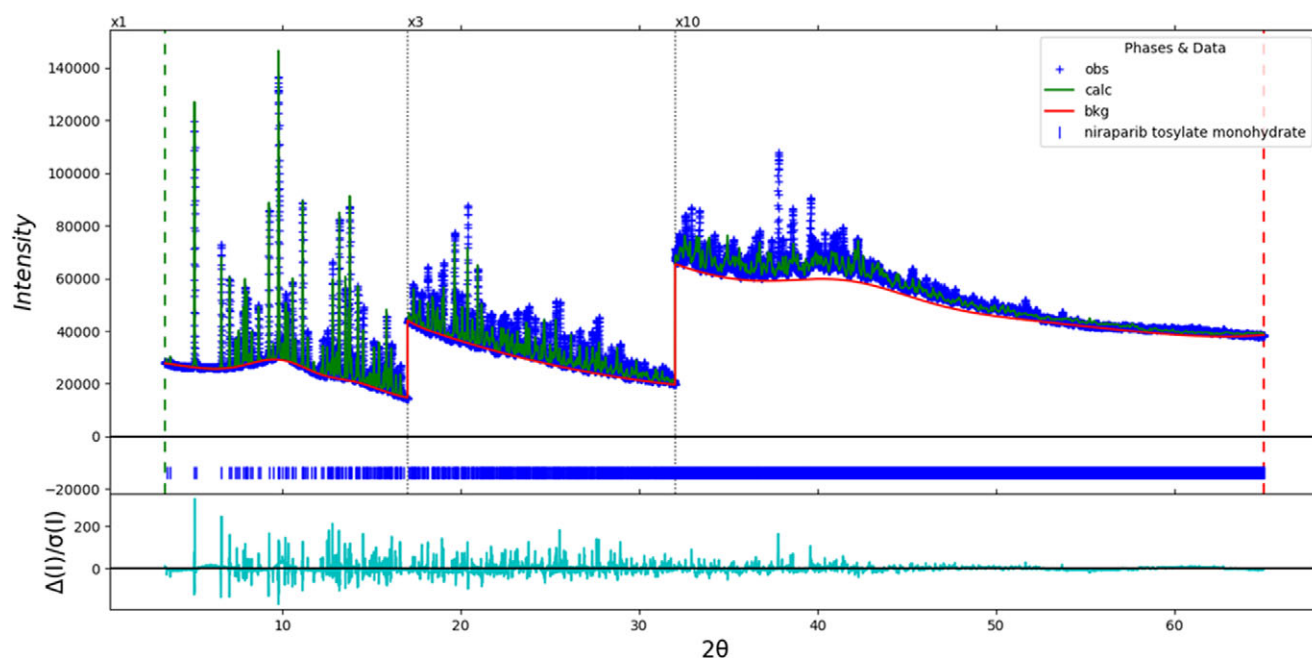


Figure 3. The Rietveld plot for the second refinement of niraparib tosylate monohydrate Form I ($R_{\text{wp}} = 0.0537$). The blue crosses represent the observed data points, and the green line is the calculated pattern. The cyan curve is the normalized error plot, and the red line is the background curve. The vertical scale has been multiplied by a factor of 3× for $2\theta > 17.0^\circ$ and by a factor of 5× for $2\theta > 36.0^\circ$.

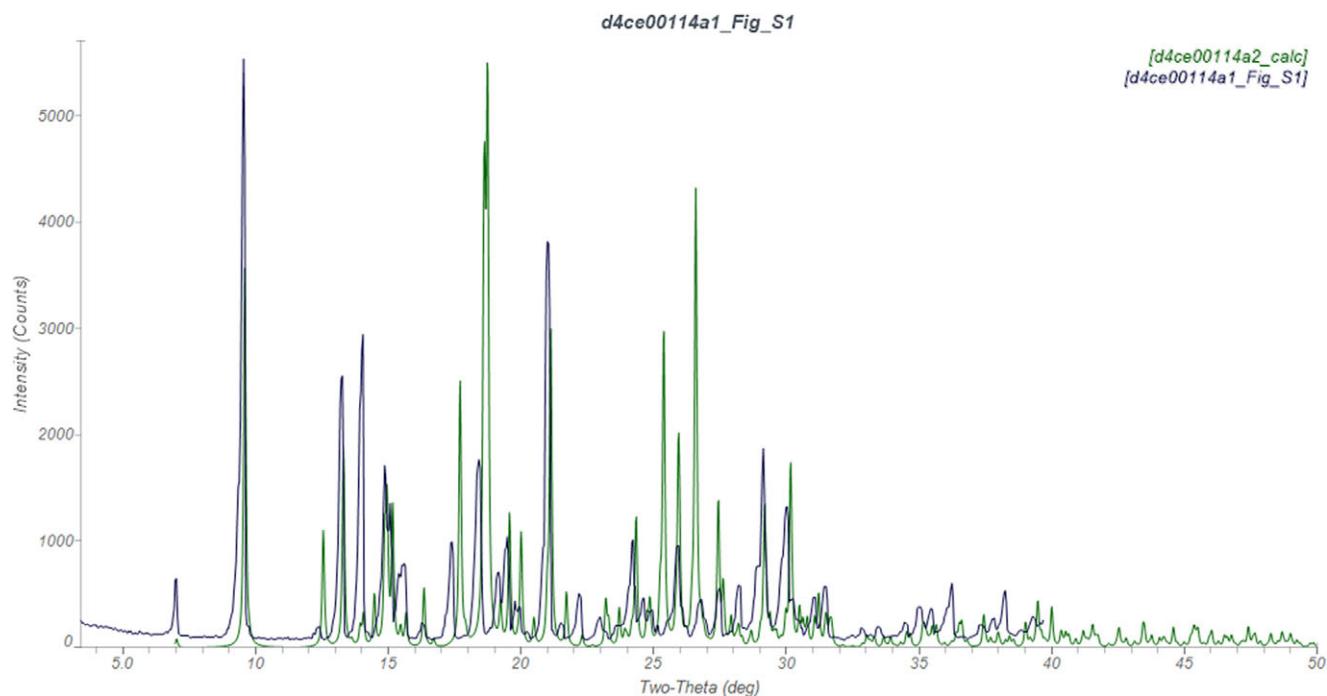


Figure 4. Comparison of the experimental powder pattern of niraparib tosylate monohydrate reported by Mudda et al. (2024) (black) with that calculated from their single-crystal structure (green). The literature pattern (measured using Cu K_{α} radiation) was digitized using UN-SCAN-IT (Silk Scientific, 2013). Image generated using JADE Pro (MDI, 2024).

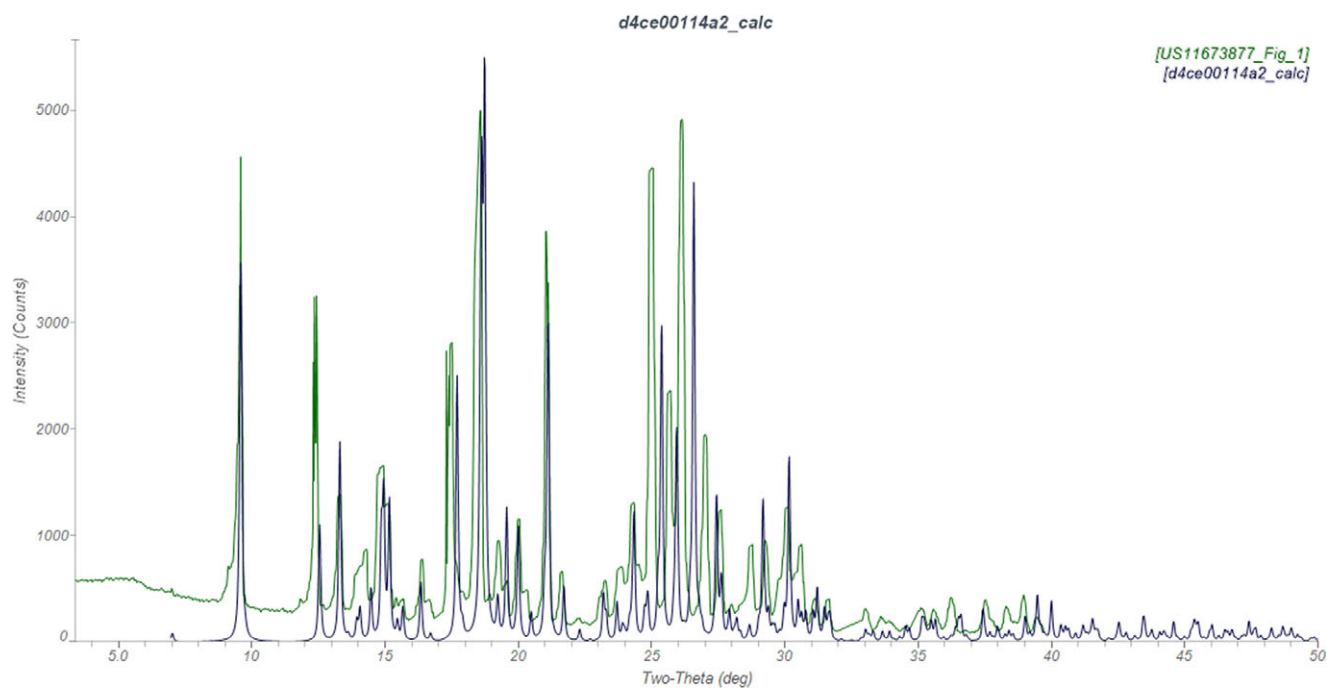


Figure 5. Comparison of the experimental powder pattern of niraparib tosylate monohydrate reported by Wu et al. (2023) (green) with that calculated from the single-crystal structure of Mudda et al. (2024) (black). The literature pattern (measured using Cu K_{α} radiation) was digitized using UN-SCAN-IT (Silk Scientific, 2013). Image generated using JADE Pro (MDI, 2024).

c -axes are 0.6% and 0.4%, respectively. The smaller unit cell at 100 K results in significant peak shifts compared with 298 K (Figure 6), meaning that the pattern calculated from the 100 K single crystal structure might not be useful for phase identification; the peak shifts may be outside the d -spacing tolerance used in the search/match methods for phase identification. As noted below, our sample exhibits a preferred

orientation, resulting in some changes in peak intensities compared to the calculated pattern.

The root-mean-square Cartesian displacement of the non-H atoms in the Rietveld-refined and VASP-optimized cations is 0.117 Å, and in the anions is 0.109 Å (Figure 7). The absolute difference in the position of the water molecule O64 is 0.300 Å. The agreement is within the normal range

TABLE I. Lattice parameters of niraparib tosylate monohydrate. Space group *P*-1

Source	Mudda et al. (2024)	This work
T, K	100(11)	298
<i>a</i> , Å	7.1123(2)	7.22060(7)
<i>b</i> , Å	12.6881(3)	12.76475(20)
<i>c</i> , Å	13.3199(3)	13.37488(16)
α , °	88.7065(17)	88.7536(18)
β , °	87.275(2)	88.0774(10)
γ , °	82.989(2)	82.2609(6)
<i>V</i> , Å ³	1,191.51(5)	1,220.650(16)

for correct structures (van de Streek and Neumann, 2014). The asymmetric unit is illustrated in Figure 8. The atom names of Mudda et al. (2024) have been used. Although the displacement coefficients of the atoms in the piperidine ring are slightly larger than those in the other fragments, the disorder noted in the single-crystal structure is not obvious. The remaining discussion will emphasize the VASP-optimized structure of our study.

All of the bond distances, bond angles, and most of the torsion angles fall within the normal ranges indicated by a Mercury Mogul Geometry check (Macrae et al., 2020). Only the C16B–C15B–C12–C11 torsion angle is flagged as unusual. This angle lies on the tail of a very broad distribution and represents the orientation of the piperidine ring with respect to the phenyl ring. Given that the piperidine ring is protonated and forms strong hydrogen bonds, we might expect the orientation of this ring to be slightly unusual.

Quantum chemical geometry optimization of the isolated cation (DFT/B3LYP/6-31G*/water) using Spartan '24 (Wavefunction, 2023) indicated that the observed conformation is 4.7 kcal/mol higher in energy than a local minimum, which has slightly different orientations of the phenyl and piperidine rings. The global minimum-energy conformation (MMFF force field) has a different orientation of the piperidine ring, showing that intermolecular interactions determine the solid-state conformation.

The crystal structure (Figure 9) consists of alternating double layers of cations and anions (including the water molecules) parallel to the *ab*-plane. Strong hydrogen bonds

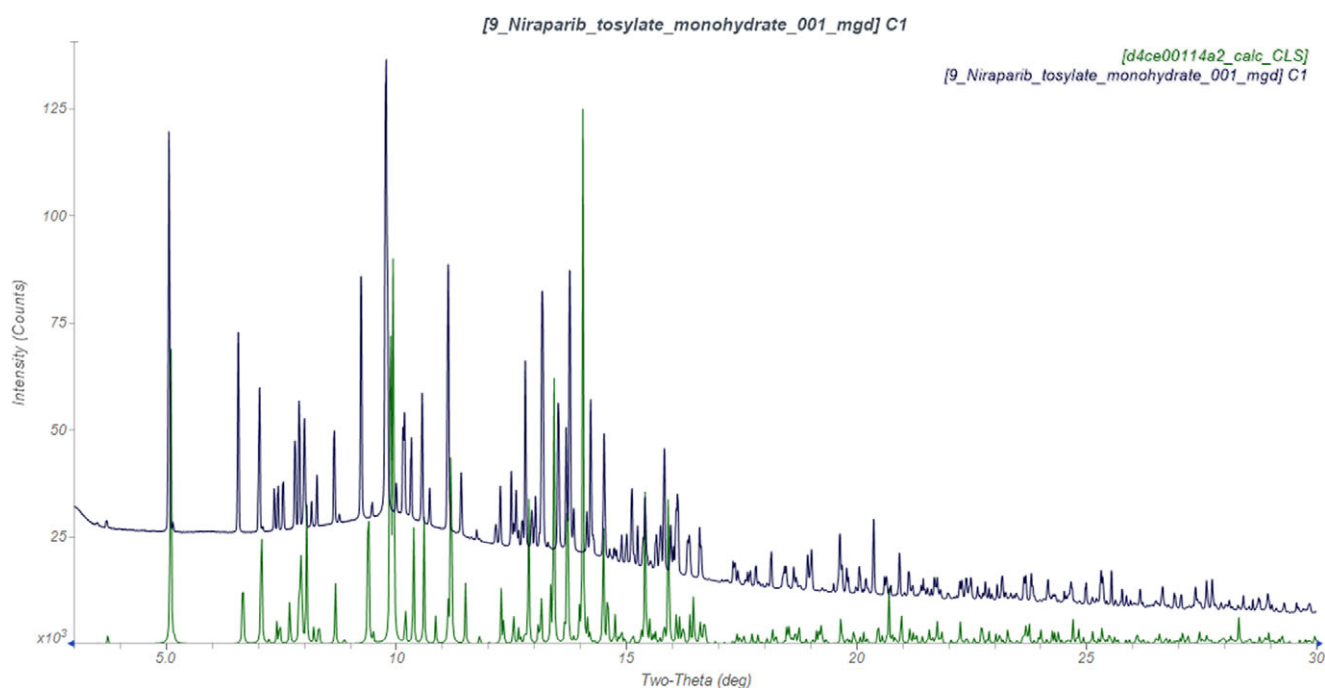


Figure 6. Comparison of the experimental synchrotron powder pattern of niraparib tosylate monohydrate Form I (298 K; black) with that calculated from the single-crystal structure of Mudda et al. (2024) (100 K; black) (calculated using the synchrotron wavelength of 0.819563(2) Å). Image generated using JADE Pro (MDI, 2024).

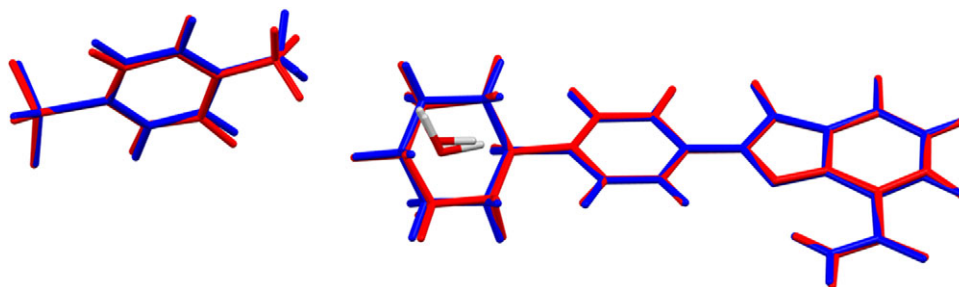


Figure 7. Comparison of the Rietveld-refined (red) and VASP-optimized (blue) structures of niraparib tosylate monohydrate Form I. The root-mean-square Cartesian displacements for the cation and the anion are 0.117 and 0.109 Å, respectively. Image generated using Mercury (Macrae et al., 2020).

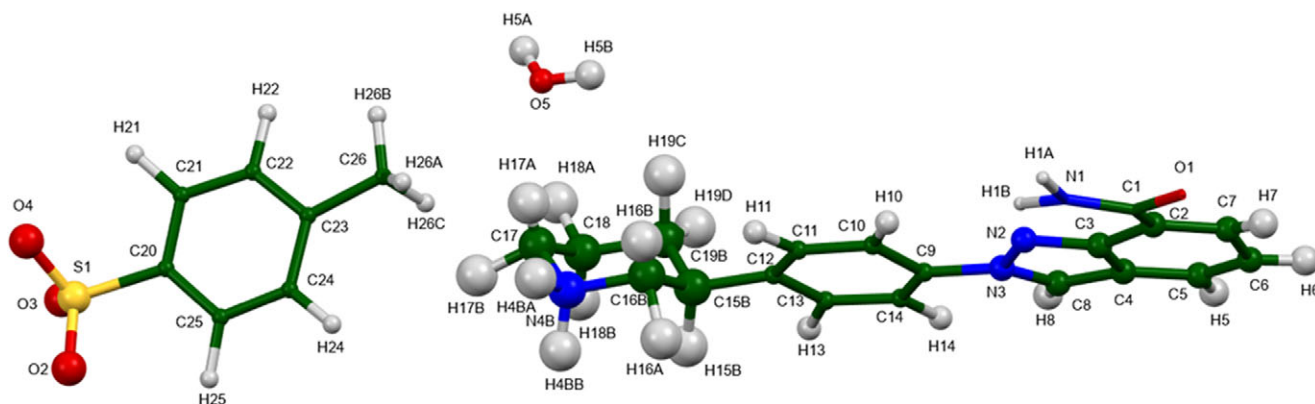


Figure 8. The asymmetric unit of niraparib tosylate monohydrate Form I, with the atom numbering. The atoms are represented by 50% probability spheroids. Image generated using Mercury (Macrae et al., 2020).

both parallel and perpendicular to the *ab*-plane link the fragments into a three-dimensional framework. The mean planes of the phenyl ring and the indazole ring system in the cation are approximately 9,7,1 and 9,6,−1, and the mean plane of the phenyl ring of the tosylate anion is approximately 0,3,7. The Mercury Aromatics Analyser indicates strong phenyl–phenyl interactions between the cations (distance = 3.63 and 3.77 Å), moderate interactions between the indazole ring systems (distance = 6.14 and 6.34 Å), and a weak phenyl–phenyl interaction of 7.77 Å. There are strong interactions between the anions (distance = 4.75 Å), as well as several weak cation–anion interactions.

Analysis of the contributions to the total crystal energy of the structure using the Forcite module of Materials Studio (Dassault Systèmes, 2023) indicates that angle distortion terms dominate the intramolecular energy, as might be expected for a molecule containing a fused ring system. The intermolecular energy is dominated by electrostatic attractions, which, in this force-field-based analysis, include hydrogen bonds. The hydrogen bonds are better discussed using the results of the density functional theory (DFT) calculation.

Hydrogen bonds are prominent in the crystal structure (Table II). The water molecule acts as a donor to two different O atoms of the tosylate anion and as an acceptor from one of

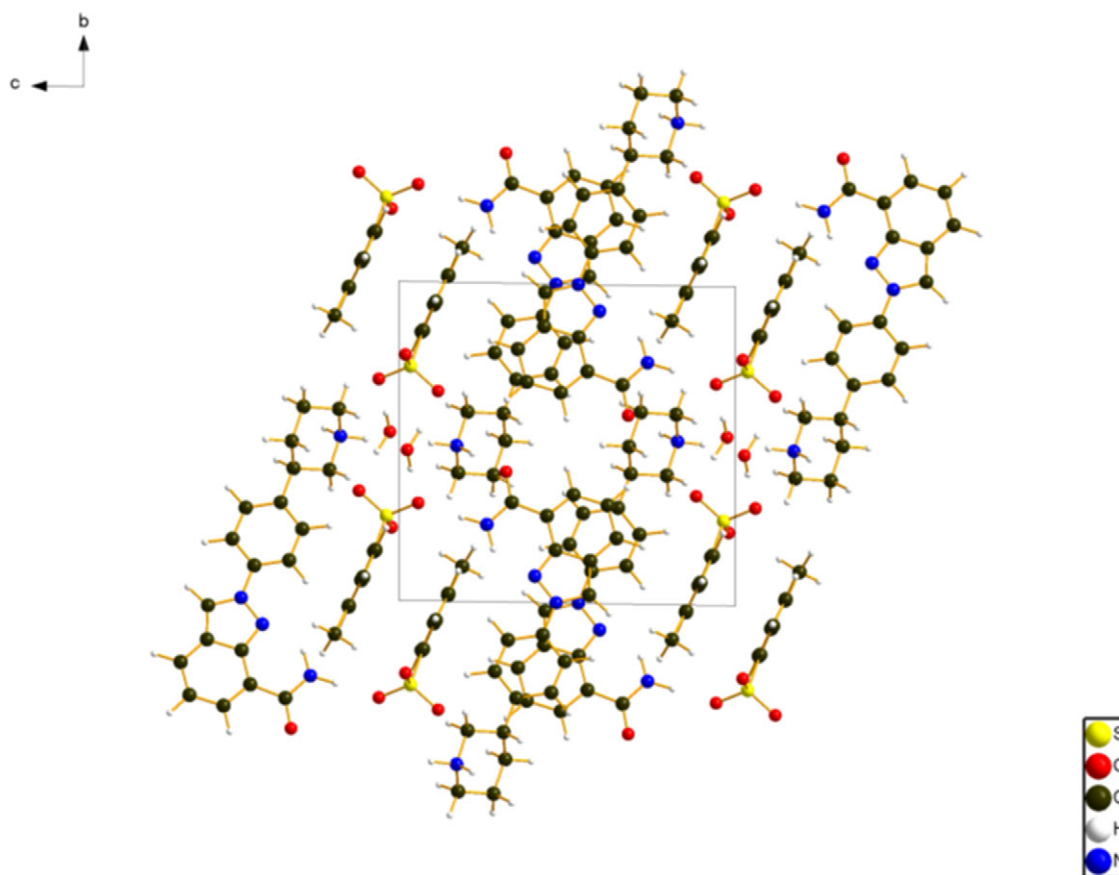


Figure 9. The crystal structure of niraparib tosylate monohydrate Form I, viewed down the *a*-axis. Image generated using Diamond (Crystal Impact, 2023).

TABLE II. Hydrogen bonds (CRYSTAL23) in the crystal structure of niraparib tosylate monohydrate. * = intramolecular.

H bond	D–H, Å	H···A, Å	D···A, Å	D–H···A, °	Overlap, <i>e</i>	<i>E</i> , kcal/mol
O5–H5A···O3	0.992	1.783	2.768	171.2	0.056	12.9
O5–H5B···O4	0.993	1.764	2.756	176.8	0.053	12.6
N4B–H4BB···O5	1.064	1.707	2.752	166.1	0.092	7.0
N4B–H4BA···O1	1.053	1.761	2.779	161.3	0.073	6.2
N1–H1A···O4	1.031	1.825	2.853	175.2	0.063	5.8
N1–H1B···N2	1.024	1.963*	2.809	138.0	0.049	–
C17–H17A···O5	1.100	2.156	3.251	173.0	0.042	–
C11–H11···O2	1.090	2.597	3.632	158.3	0.015	–
C16B–H16A···O3	1.098	2.715	3.612	138.5	0.010	–
C10–H10···N2	1.087	2.460*	2.813	97.3	0.011	–
C7–H7···O1	1.091	2.440*	2.813	98.3	0.011	–
C24–H24···N1	1.090	2.581	3.662	170.6	0.012	–
C22–H22···O2	1.090	2.668	3.466	129.5	0.010	–

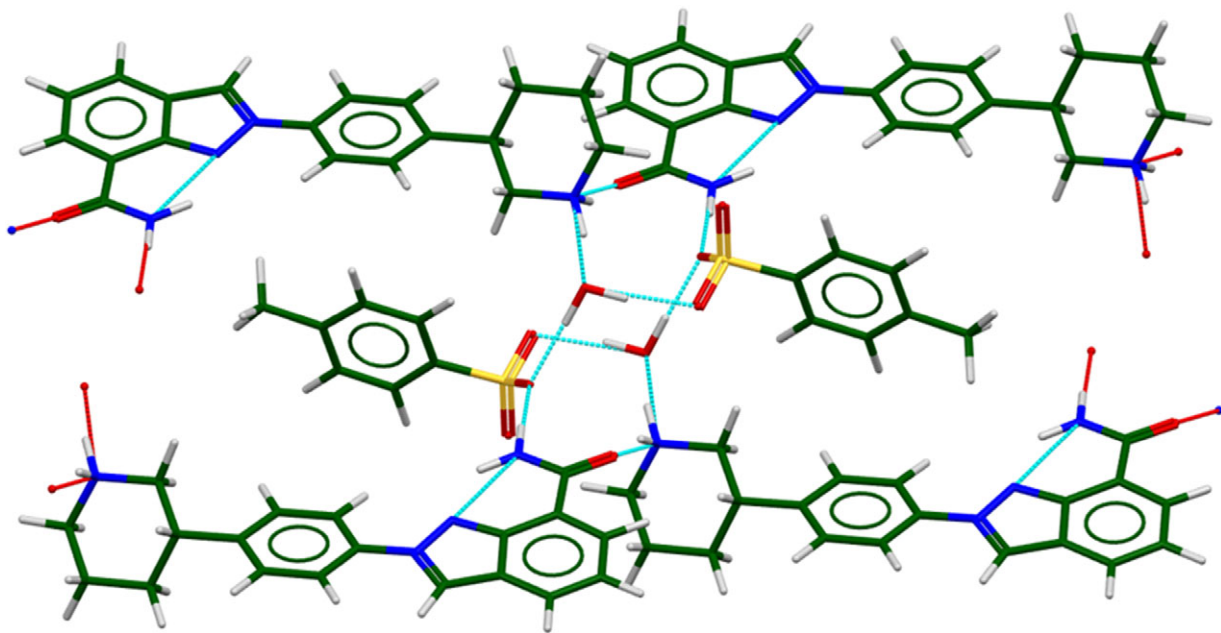


Figure 10. The hydrogen-bonded clusters of niraparib cations, tosylate anions, and water molecules. Image generated using Mercury (Macrae et al., 2020).

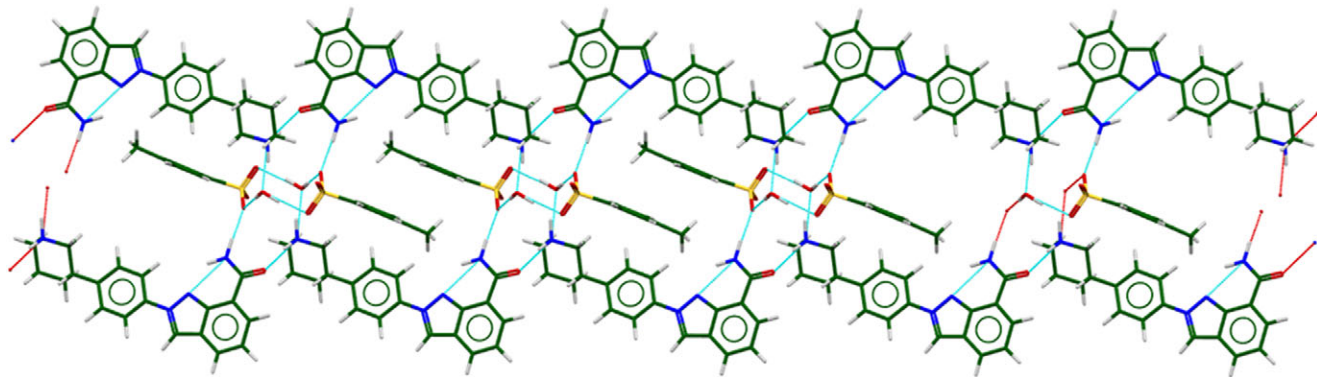


Figure 11. The complex hydrogen-bonded chains along the *b*-axis in niraparib tosylate monohydrate Form I. Image generated using Mercury (Macrae et al., 2020).

the H atoms of the protonated piperidine ring. The other piperidyl N–H acts as a donor to the carbonyl group of another cation. Surprisingly, there are no cation–anion N–H···O hydrogen bonds. The amide group forms as a N–H···O

hydrogen bond to the anion and an intramolecular N–H···N hydrogen bond to the indazole ring. The energies of the O–H···O hydrogen bonds were calculated using the correlation of Rammohan and Kaduk (2018) and the energies of the

N–H...O hydrogen bonds using the correlation of Wheatley and Kaduk (2019). The hydrogen bonds form the piperidine ring and amide groups link four cations, two anions, and two water molecules into a cluster (Figure 10). Similar links from the other ends of the cations result in a complex chain along the *b*-axis (Figure 11), and these chains link to form a three-dimensional hydrogen-bonded framework. There are C–H...O hydrogen bonds between the cation and the anion and C–H...O and C–H...N hydrogen bonds between the anion and the cation.

As noted above, the Bravais–Friedel–Donnay–Harker (Bravais, 1866; Friedel, 1907; Donnay and Harker, 1937) algorithm suggests that we might expect elongated morphology for niraparib tosylate monohydrate, with $\langle 010 \rangle$ as the long axis. A fourth-order spherical harmonic model was included in the refinement. The texture index was 1.050(1), indicating that preferred orientation was slight in this rotated capillary specimen.

IV. CONCLUSIONS

Monte Carlo simulated annealing techniques yielded a crystal structure for niraparib tosylate monohydrate Form I. The usual analysis of short contacts (potential hydrogen bonds) suggested protonation of the cation at the amide group, which would be a surprise. This structure agreed with its DFT-optimized version within the normal range for correct structures. A substructure search in the Cambridge Structural Database (CSD) indicated that only three protonated phenyl amide structures have been reported; therefore, protonation there would be highly unusual. Fortunately, as we began writing this paper, a crystal structure for niraparib tosylate monohydrate was reported, with the cation protonated as expected on the piperidine ring. The two structures fit the data equally well ($R_{wp} = 0.0537$). This is not unreasonable, as they differ only in the position of one hydrogen atom. Protonation at the piperidine ring yields a lower-energy structure, so is to be preferred. Interpretation of the original structure was confounded by the facts that the expected N–H...O hydrogen bonds between a protonated N and the anion are not present and that the neutral amide acts as a hydrogen bond donor to the anion. Therefore, chemical reasonableness (Kaduk, 2019) can be even more important than statistical and graphical measures of the fit, but one must be ready to be surprised.

DATA AVAILABILITY STATEMENT

The powder pattern of niraparib tosylate monohydrate from this synchrotron dataset has been submitted to the International Centre for Diffraction Data (ICDD) for inclusion in PDF[®]. The Crystallographic Information Framework (CIF) files containing the results of the Rietveld refinement (including the raw data) and the DFT geometry optimization were deposited with the ICDD. The data can be requested at pdj@icdd.com.

ACKNOWLEDGEMENTS

Part of the research described in this paper was performed at the Canadian Light Source, a national research facility of the University of Saskatchewan, which is supported by the Canada Foundation for Innovation (CFI), the Natural Sciences and

Engineering Research Council (NSERC), the Canadian Institute of Health Research (CIHR), the Government of Saskatchewan, and the University of Saskatchewan. This work was partially supported by the International Centre for Diffraction Data. We thank Adam Leontowich for his assistance in the data collection. We also thank the ICDD team – Megan Rost, Steve Trimble, and Dave Bohnenberger – for their contribution to research, sample preparation, and in-house XRD data collection and verification.

CONFLICTS OF INTEREST

The authors have no conflicts of interest to declare.

REFERENCES

- Altomare, A., C. Cuocci, C. Giacovazzo, A. Moliterni, R. Rizzi, N. Corriero, and A. Falcicchio. 2013. "EXPO2013: A Kit of Tools for Phasing Crystal Structures from Powder Data." *Journal of Applied Crystallography* 46: 1231–5.
- Bravais, A. 1866. *Etudes Cristallographiques*. Paris: Gauthier Villars.
- Bruno, I. J., J. C. Cole, M. Kessler, J. Luo, W. D. S. Motherwell, L. H. Purkis, B. R. Smith, et al. 2004. "Retrieval of Crystallographically-Derived Molecular Geometry Information." *Journal of Chemical Information and Computer Sciences* 44: 2133–44.
- Crystal Impact. 2023. *Diamond V. 5.0.0*, edited by H. Putz & K. Brandenburg. Bonn: Crystal Impact.
- Dassault Systèmes. 2023. *BIOVIA Materials Studio 2024*. San Diego, CA: BIOVIA.
- Donnay, J. D. H., and D. Harker. 1937. "A New Law of Crystal Morphology Extending the Law of Bravais." *American Mineralogist* 22: 446–7.
- Erba, A., J. K. Desmarais, S. Casassa, B. Civalleri, L. Donà, I. J. Bush, B. Searle, et al. 2023. "CRYSTAL23: A Program for Computational Solid-State Physics and Chemistry." *Journal of Chemical Theory and Computation* 19: 6891–932; <https://doi.org/10.1021/acs.jctc.2c00958>.
- Friedel, G. 1907. "Etudes sur la loi de Bravais." *Bulletin de la Société Française de Minéralogie* 30: 326–455.
- Gatti, C., V. R. Saunders, and C. Roetti. 1994. "Crystal-Field Effects on the Topological Properties of the Electron-Density in Molecular Crystals – the Case of Urea." *Journal of Chemical Physics* 101: 10686–96.
- Groom, C. R., I. J. Bruno, M. P. Lightfoot, and S. C. Ward. 2016. "The Cambridge Structural Database." *Acta Crystallographica Section B: Structural Science, Crystal Engineering and Materials* 72: 171–9.
- Kabekkodu, S., A. Dosen, and T. N. Blanton. 2024. "PDF-5+: A Comprehensive Powder Diffraction File™ for Materials Characterization." *Powder Diffraction* 39: 47–59.
- Kaduk, J. A. 2019. "Chapter 4.9: Structure Validation." In *International Tables for Crystallography Volume H: Powder Diffraction*, edited by C. J. Gilmore, J. A. Kaduk and H. Shenk, 489–514. Chester: International Union of Crystallography.
- Kaduk, J. A., C. E. Crowder, K. Zhong, T. G. Fawcett, and M. R. Suchomel. 2014. "Crystal Structure of Atomoxetine Hydrochloride (Strattera), C₁₇H₂₂NOCl." *Powder Diffraction* 29: 269–73.
- Kim S., J. Chen, T. Cheng, A. Gindulyte, J. He, S. He, Q. Li, et al. 2023. "PubChem 2023 Update." *Nucleic Acids Research* 51 (D1): D1373–D1380. <https://doi.org/10.1093/nar/gkac956>.
- Kresse, G., and J. Furthmüller. 1996. "Efficiency of Ab-Initio Total Energy Calculations for Metals and Semiconductors Using a Plane-Wave Basis Set." *Computational Materials Science* 6: 15–50.
- Leontowich, A. F. G., A. Gomez, B. Diaz Moreno, D. Muir, D. Spasyuk, G. King, J. W. Reid, C.-Y. Kim, and S. Kycia. 2021. "The Lower Energy Diffraction and Scattering Side-Bounce Beamline for Materials Science at the Canadian Light Source." *Journal of Synchrotron Radiation* 28: 1–9. <https://doi.org/10.1107/S1600577521002496>.
- Macrae, C. F., I. Sovago, S. J. Cottrell, P. T. A. Galek, P. McCabe, E. Pidcock, M. Platings, et al. 2020. "Mercury 4.0: From Visualization to Design and Prediction." *Journal of Applied Crystallography* 53: 226–35.
- Materials Design. 2024. *Medea 3.7.2*. San Diego, CA: Materials Design Inc.
- MDI. 2024. *JADE Pro Version 9.0*. Livermore, CA: Materials Data.

- Mudda, R. R., R. Devarapalli, A. Das, P. R. Lakkireddy, C. M. Reddy, and R. Chennuru. 2024. "A Zwitterionic Salt-Cocrystal: in vitro Insights from Niraparib Tosylate, an Anti-Cancer Drug." *CrystEngComm* 26: 2463–73.
- Peintinger, M. F., D. Vilela Oliveira, and T. Bredow. 2013. "Consistent Gaussian Basis Sets of Triple-Zeta Valence with Polarization Quality for Solid-State Calculations." *Journal of Computational Chemistry* 34: 451–9.
- Rammohan, A., and J. A. Kaduk. 2018. "Crystal Structures of Alkali Metal (Group 1) Citrate Salts." *Acta Crystallographica Section B: Crystal Engineering and Materials* 74: 239–52.
- Silk Scientific. 2013. *UN-SCAN-IT 7.0*. Orem, UT: Silk Scientific Corporation.
- Stephens, P. W. 1999. "Phenomenological Model of Anisotropic Peak Broadening in Powder Diffraction." *Journal of Applied Crystallography* 32: 281–9.
- Stewart A. J., Y. Wang, G. Wu, and J. Yin. 2020. "Crystalline Forms of Niraparib Free Base." International Patent Application WP2020/072796 A1.
- Stirk, A. J., F. E. S. Souza, A. Karadeolian, and A. W. Rey. 2021. "Crystalline Forms of Niraparib Tosylate." United State Patent Application 2021/0017151 A1.
- Sykes, R. A., P. McCabe, F. H. Allen, G. M. Battle, I. J. Bruno, and P. A. Wood. 2011. "New Software for Statistical Analysis of Cambridge Structural Database Data." *Journal of Applied Crystallography* 44: 882–6.
- Toby, B. H., and R. B. Von Dreele. 2013. "GSAS II: The Genesis of a Modern Open-Source All Purpose Crystallography Software Package." *Journal of Applied Crystallography* 46: 544–9.
- van de Streek, J., and M. A. Neumann. 2014. "Validation of Molecular Crystal Structures from Powder Diffraction Data with Dispersion-Corrected Density Functional Theory (DFT-D)." *Acta Crystallographica Section B: Structural Science, Crystal Engineering and Materials* 70: 1020–32.
- Wavefunction, Inc. 2023. *Spartan '24. V. 1.0.0*. Irvine, CA: Wavefunction, Inc.
- Wheatley, A. M., and J. A. Kaduk. 2019. "Crystal Structures of Ammonium Citrates." *Powder Diffraction* 34: 35–43.
- Wu, G., J. Chaber, A. E. McKeown, and J. R. Foley. 2023. "Niraparib Compositions." U.S. Patent 11673877 B2.